94-247

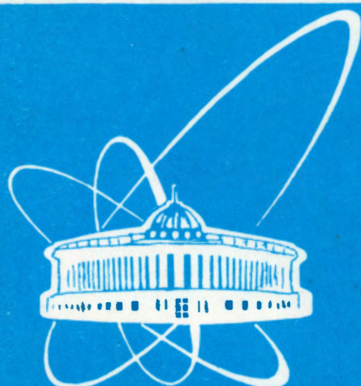

объединенный
институт
ядерных
исследований
дубна

E13-94-247

INVESTIGATION OF SILICON PLANAR DETECTORS FOR LHC PROJECT

Submitted to «Nuclear Instruments and Methods»

1994

1. Introduction

The design of detection systems for high energy physics has been widely discussed recently in connection with the future supercollider experiments (SSC and LHC) /1/. Silicon calorimetry has a sufficient capability to meet the most rigorous requirements of the projects. The calorimeter includes both: the sampling layers of detectors manufactured of high resistivity silicon and absorbing medium. The peculiarities of the detectors are:

- the total depletion at rather low bias voltage(V_d<100 V);
- a large number of the detectors (up to 5×10^6) with identical parameters is required because of the large total area occupied by the calorimeters, hence, planar technological performance is necessary;
- collection time for the both types of charge carriers (electrons and holes) less than 20 nsec.

A large R&D work has been carried out to investigate the radiation hardness of the detectors /2,3,4/ as soon as high neutron fluences are expected in supercolliders. This paper deals with the research of non-irradiated detectors including some properties of the starting silicon. The characteristics of irradiated detectors will be published separately.

2. The Experimental Technique

The detectors were produced by Research and Production Association ELMA, Russia. They represent p^{+}-n-n^{+} structures on wafers with diameter 100mm (Wacker) and 76mm (ZTMF, Zaporojie Titanium Magnesium Factory, Zaporojie, Ukraine) manufactured of the float-zone n-type-conductivity silicon. The wafer thickness was 400μm. The following processes were used while detector manufacturing: dry oxidation at the temperature of 1100°C, phosphorus diffusion or implantation to the wafer back side, thin oxidation, ion implantation of boron through the thin oxide film at the wafer front side, thermal treatments at the temperature 600°C and 860°C, aluminium

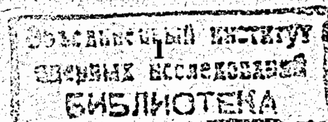
Объединенный институт ядерных исследований БИБЛИОТЕКА

double side metallization. Both: double implantation and diffusion-implantation (B, P) technology were applied. The detector topology is shown in Fig.1.

In our research the following experimental methods were applied:

- current-voltage dependence measurements;
- measurements of deep levels in the forbidden gap of silicon by Deep Level Transient Spectroscopy (DLTS);
- Hall effect measurements with special satellite samples;
- α-particle high precision spectroscopy;
- Transient Current Technique (TCT) with α-particles and gallium-arsenide (GaAs) laser pulse excitation.

3. Investigation of Silicon Crystals

Two types of the undoped float-zone silicon crystals produced by Wacker Chemitronics and ZTMF, were investigated. The crystals were of good uniformity and had the following parameters for ZTMF and Wacker silicon, respectively: the resistivity $\rho = 2.5 \div 3.0$ kOhm×cm and $4 \div 5.4$ kOhm×cm; the lifetime of the minority charge carriers $\tau_p \simeq 1.0$ ms and 4.3 ms. Selective etching in the modified Sirtl etchant have revealed that both: the ZTMF and Wacker crystals were free of dislocations and swirl-defects. One could observe only small shallow etch pits which are homogeneously distributed (Fig.2) and corresponding to the so-called D-defects (vacancy voids) /5/.

It is known that structural microdefects serve as sinks for contaminations. The fast diffusing impurity precipitation at the microdefects increases the size of the both microdefects and etch pits. At the surface (111) of the Wacker crystals the etch pits can be detected only by Nomarsky interference contrast, while in the ZTMF crystals the etch pits are visible under the optical metallographic microscope. It should be noted that the concentration of D-defects can be estimated by transmission electron microscopy and is found to be $10^{13} \div 10^{14}$ cm^{-3} /6/.

The Hall effect measurements provide an additional information on the crystal performance. The concentration n of free charge carriers and its temperature dependences are presented in Fig.3. The curve for Wacker silicon is well fitted by the linear dependence with single activation energy $E_a = E_c - 45.6$ meV corresponding to phosphorus impurity, the concentration is 9×10^{11} cm^{-3}. The concentration of compensating acceptor centres is much lower and equals to 4×10^{10} cm^{-3}. For ZTMF silicon the curve is approximated by the energy level $E_c - 36$ meV with the concentration of $3\times10^{13} cm^{-3}$ which is close to the concentration of these compensating centres. It implies that the $E_c - 36$ meV level can be attributed to some acceptor centre in the upper half of the forbidden gap providing compensation only at low temperatures. The origin of the centre is, probably, connected with the microdefect decoration phenomenon.

4. Current-Voltage Characteristics Analysis

The both technologies of detector manufacturing provide similar values of the reverse current I_r. The distribution of reverse currents for the set of detectors from Wacker silicon is shown in Fig.4. The chosen bias voltage exceeds the depletion voltage of 50 V, for the typical impurity concentration about 4×10^{11} cm^{-3} determined from the detectors capacitance-voltage characteristics as well as the possible variations of V_d in the range of 50÷80 Volts. The typical current-voltage and capacitance-voltage characteristics of detectors are shown in Fig.5.

The reverse current-voltage characteristics of the planar diode are described by the equation including three components: the diffusion current, bulk generation, and surface generation at the Si-SiO_2 interface under the aluminium overlapping electrode:

$$I_r = \frac{e p_{no}}{\tau_p}(d - W) + \frac{e n_i W A}{\tau_{eff}} + e n_i S_g A_{ox} \qquad (1)$$

where:

e – electron charge;

p_{no} – hole concentration in the neutral base region;

n_i – intrinsic carrier concentration;

τ_{eff} – effective generation lifetime;

S_g – generation rate at the $Si\text{-}SiO_2$ interface;

d – sample thickness;

W – thickness of the space charge region (SCR);

A – p^+-n junction area;

A_{ox} – area under the aluminium overlapping electrode.

The current-voltage characteristics of the detectors and the temperature dependence of the current are shown in Fig.6,7. To analyze the dependences and estimate the lifetimes, the additional experiments have been carried out:

- manufacturing of the detectors with small area (0.25 cm^2);
- investigation of the deep levels by DLTS-method;
- the measurements of the forward current-voltage characteristics.

The reverse current-voltage characteristic of the detector with a small area (Fig.6) represents the contribution of the surface generation current at the $Si\text{-}SiO_2$ interface as a sharp increase of the current at V_{bias} = 2÷3 V. The estimation of the surface generation velocity S_g yields 60 cm/sec, small enough to influence the reverse current of the large area detectors with A = 4 cm^2. For the majority of the detectors with I_r < 50 nA the current is determined by the bulk generation component, I_r is proportional to $\sqrt{V_{bias}}$ in the range below the depletion voltage. The slope of the reverse current temperature dependence (Fig.7) is defined by the activation energy of 0.7eV for the bias below and over the full depletion voltage, the reasons are not quite clear up to now.

DLTS spectra (Fig.8) have shown that two deep levels

with the following parameters are induced by the thermal treatment while detector manufacturing:

DL1: $E_a = E_c - 0.56$ eV, $\sigma_n = 3\times10^{-15}$ cm^2;

DL2: $E_a = E_c - 0.26$ eV, $\sigma_n = 7\times10^{-18}$ cm^2;

where σ_n is the electron capture cross-section. The deep levels are typical thermal defects /7,8/ induced in silicon if the temperature exceeds 1000°C. The deep level DL1 is an effective generation centre with the concentration N_t in the range of $(3\times10^8 \div 4\times10^{10})$ cm^{-3}. In the assumption that the hole capture cross-section $\sigma_p \gg \sigma_n$ (it follows from the negligible value of DLTS peaks for the lower half of the forbidden gap), one can estimate the generation lifetime $\tau_g = (v_{th} N_t \sigma_n)^{-1}$, where v_{th} is the thermal electron velocity. The obtained values are compared in Table 1, where the current densities J and effective generation lifetimes τ_{eff} have been calculated from current-voltage dependences.

The presented data have shown a good correlation of the reverse current and deep level concentration. We suppose τ_{eff} = 100 ms to be the upper limit of the generation lifetime.

As for detectors with I_r > 50 nA, there are deep levels induced occasionally in the lower half of the forbidden gap. One of them has the enlarged value of $\sigma_n \simeq 10^{-12}$ cm^2, hence, the generation via this centre may increase the reverse current essentially.

Recombination lifetime τ_r (equivalent to τ_p) is determined from the forward current-voltage characteristics. The main advantage of it is that the forward current (I_f) as the exponential function of the voltage is more stable and has a small sensitivity to the leakages. The forward current density J_f at a low injection level is found as

$$J_f = J_s \left[\exp\left(\frac{eV}{\beta kT}\right)\right] \qquad (2)$$

with

$$J_s = \frac{en_i^2 D_p}{N_D L_p} \times \frac{S_r ch(d/L_p) + (D_p/L_p) sh(d/L_p)}{(D_p/L_p) ch(d/L_p) + S_r sh(d/L_p)} \quad (3)$$

and $L_p = \sqrt{(D_p \tau_r)}$,

where:

J_s - the saturation current density;

β - the numerical factor;

k - the Boltzmann constant;

T - the absolute temperature;

L_p and D_p - the diffusion length and the diffusion coefficient of holes, respectively;

S_r - surface recombination velocity for n-n^+ boundary;

N_D - the effective impurity concentration in n-Si.

It is possible to estimate only either $\tau_{r\,max}$ ($S_r \rightarrow 0$) or $S_{r\,max}$ ($\tau_r \rightarrow \infty$):

$$J_s(L_p/d,\ 0) = (en_i^2/N_D)\times(D_p/L_p)th(d/L_p) \quad (3a)$$

$$J_s(\infty,\ S_r) = (en_i^2/N_D)\times S_r D_p/(S_r d + D_p) \quad (3b)$$

The typical experimental dependences of $I_f = J_f \times A$ versus V_f for detectors with different τ_r, are presented in Fig.9. The exponential factor β is equal to 1, so the current is dominated by the diffusion of the minority charge carriers. According to equation (3b) the value of S_{rmax} does not exceed 10 cm/sec.

The correlation plot between the reverse current and recombination lifetime for the set of detectors with area $A = 4\ cm^2$, presented in Fig.10, reveals a tendency of the reverse current to grow with the recombination lifetime decreasing.

The comparison of the calculated and experimental ratios I_r/I_f allows one to define the origin of the currents. The experimental values of the reverse and forward currents have been measured at the reverse bias voltage of 3.0 V and at the forward bias voltage of 0.1 V, respectively. The experimental ratio equals to 0.11÷0.17 while the calculated one is $0.2\times(\tau_r/\tau_g)$ with $\tau_r = \tau_{po}$ and $\tau_g = \tau_{po}\exp[(E_a - E_i)/kT] + \tau_{no}\exp[(E_i - E_a)/kT]$, where E_i is the middle of the forbidden gap. The estimation reveals that the recombination and generation of the charge carriers take place via the centres in the middle of the forbidden gap.

5. Transport Phenomena Investigation

The detectors manufactured at ELMA with small values of the reverse current and capacitance (about 100 pF for the totally depleted structures) are perspective ones for the high precision spectroscopy of the accelerated ions and charged particles.

The measurements of the detector characteristics such as the noise level, energy resolution and amplitude deficiency, have been carried out using the ORTEC spectrometry facility (the intrinsic noise level about 1.7 keV). The method of precise measurements of the amplitude deficiency with the reference detector, has been applied in our tests and was described [9]. The obtained accuracy was 10^{-4}.

The measurements of the amplitude deficiency as a function of the reverse bias voltage and detector tilting angle, have shown the deficiency to be mainly affected by the thickness of the detector entrance window and is equal to 2.5÷3.0%. The value corresponds to the thickness of 1.0÷1.2 μm including the aluminium contact film and dead layer d_{dead} (the pre-surface part of high doped p^+-layer or n^+-layer if the back surface is irradiated with α-particles).

The measured dead layer of 2000Å is by two times more than the average dead layer thickness of the spectrometry detectors manufactured with the ion implantation technology [10].

The amplitude deficiency determined by the charge

collection of the non-equilibrium charge carriers equals to 10^{-3} in the bias voltage range of $V = 50 \div 200$ V for the electrons and $V > V_d$ for the holes. The negligible value of the amplitude deficiency indicates that there are no trapping phenomena for the non-equilibrium carriers in the space charge region.

The signal kinetics of the detectors is represented by the current response curves for different types of excitation:

- α-particles (Fig.11);
- intensively absorbed light pulse of gallium-arsenide laser with 0.83 μm wave length and light pulse duration - 0.7 ns (Fig.12);
- minimum ionizing particles (m.i.p., Fig.13).

It should be emphasized that the pulse duration is connected with the drift time of the proper charge carriers i.e. their mobility and the average electric field. For α-particles there is an additional contribution to the response pulse duration dependent on the electric field and plasma stage. Thus, some features of the electric field distribution are hidden especially for the fast process of the electrons drift (α-particle irradiation of p^+-layer, Fig.11,a).

One can estimate the drift time as $t_d \simeq d/v_d$ (v_d is the drift velocity) - for detector thickness $d = 400$ μm, the drift time for electrons $t_d \cong 4$ ns, whereas the plasma time equals $\simeq 5$ ns at the detector biased by 160 Volts and the average electric field about 4 kV/cm /11/.

In our experiments the best time resolution and plasma effect elimination have been provided with the laser light pulse excitation of the non-equilibrium charge carriers. The other advantage of this experimental version is the possibility to obtain the current pulse response without any signal preamlification. Some parameters of the employed facility are:

- light pulse duration of GaAs laser $\simeq 0.7$ ns;
- effective pulse energy ≤ 100 MeV;
- area of light spot $\geq 400 \times 400 \mu m^2$;
- time resolution of oscilloscope 200 ps.

For partially depleted detectors the electron component of the pulse response has an exponential decreasing(Fig.12,a) while the hole component is small and has a large duration (Fig.12,b) due to the hole diffusion in the neutral base region. When the detectors are fully depleted the pulse curves do not show any slow component (Fig.12,c,d) which arises if the charge carriers trapping-detrapping takes place.

If the relativistic particles are detected, the both types of charge carriers are generated homogeneously along the particle tracks in the space-charge region of the detectors. It leads either to the deficiency and pulse duration decreasing in comparison with the surface light pulse absorption, or α-particle generation of the non-equilibrium charge carriers. Indeed, for the m.i.p. excitation the pulse duration is approximately 20 ns for the fully depleted detector (Fig.13).

To analyze the alternative possibilities of the detector application, the measurements of the energy resolution δ_α (α-particles of ^{210}Po) and the noise level δ_N of the fully depleted detectors have been carried out (Table 2).

The noise level seems to be acceptable, as for the energy resolution aiming the high precision spectroscopy, it is necessary to decrease or delete entirely the aluminium film and diminish the thickness of p^+-layer by means of lowering the ion imlantation energy .

The detectors modified in such a way are promising to be applied in the ion beam diagnostics of materials as well as in the analysis of the radioactive isotope mixtures.

Table 1

Comparison of the reverse current density and deep level concentration

J, $nA/cm^2/100\ \mu m$	τ_{eff}, ms	N_t, cm^{-3}	τ_g, ms
0.2	≈100	$\le 3\times10^{8}$	≥ 100
1.5	23	1×10^{9}	30
8.0	3	4×10^{10}	0.8

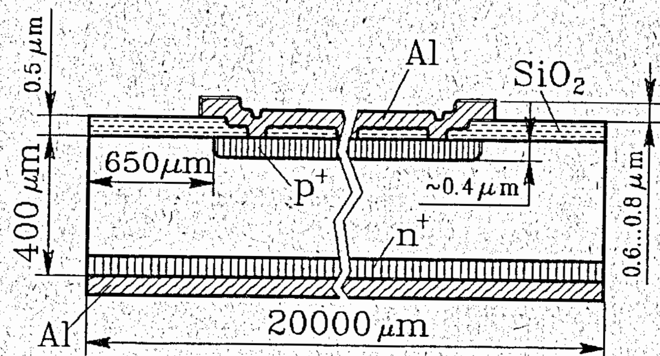

Fig.1 The detector lay-out.

Table 2

The noise level and energy resolution of the detectors

A, cm^2	δ_α, keV	δ_N, keV
0.25	16.5	6.5
4.0	30÷33	9÷12

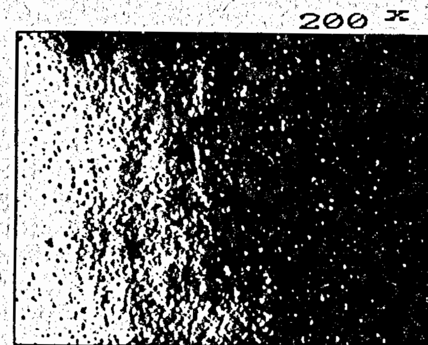

Fig.2 Distribution of etching pits on [111] plane of Wacker silicon crystal after Sirtl etching.

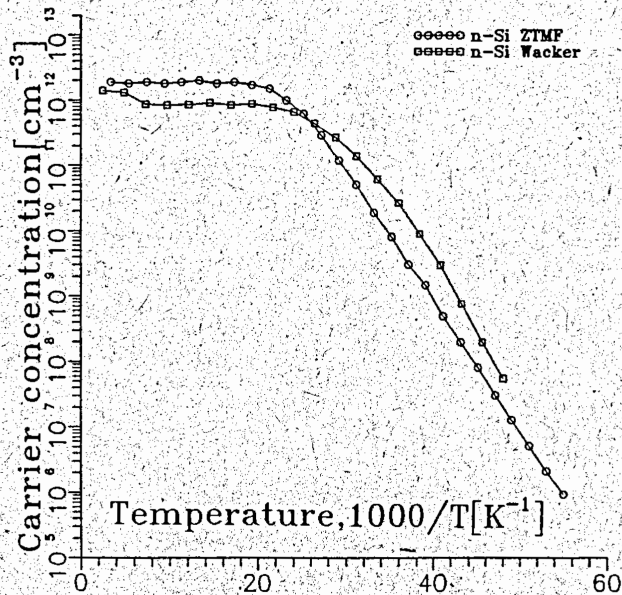

Fig.3 Temperature dependence of the free carriers concentration for Wacker and ZTMF silicon samples.

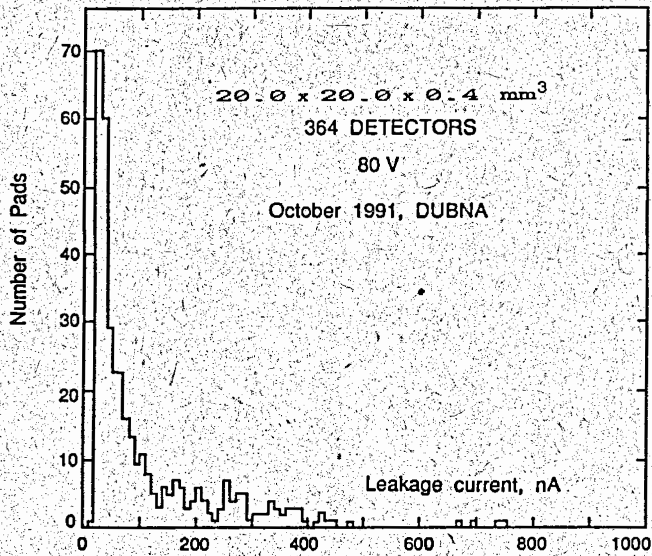

Fig.4 Distribution of reverse currents for the set of detectors made of Wacker silicon. The area is 4 cm^2, U_{bias} = 120 Volts.

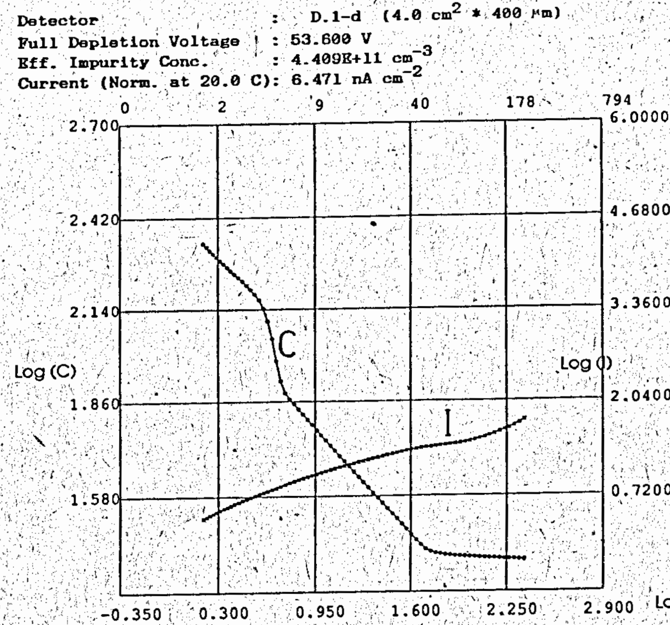

Fig.5 Typical reverse current-voltage and capacitance-voltage characteristics of detectors made of Wacker silicon. The area is 4 cm^2.

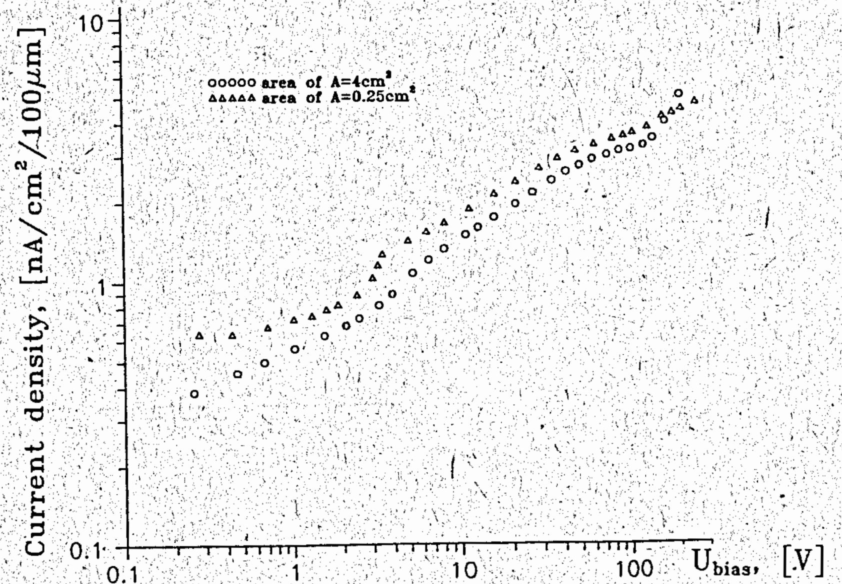

Fig.6 Reverse current-voltage characteristics of detectors with different areas.

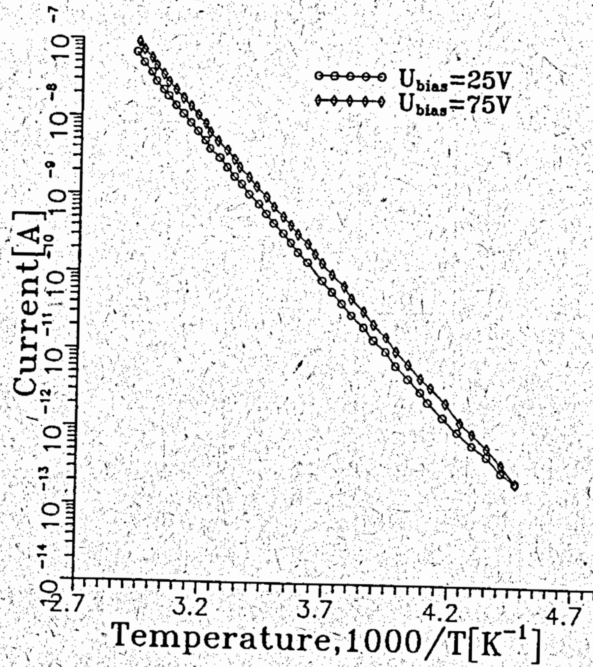

Fig.7 Temperature dependence of the reverse current at different bias voltages.

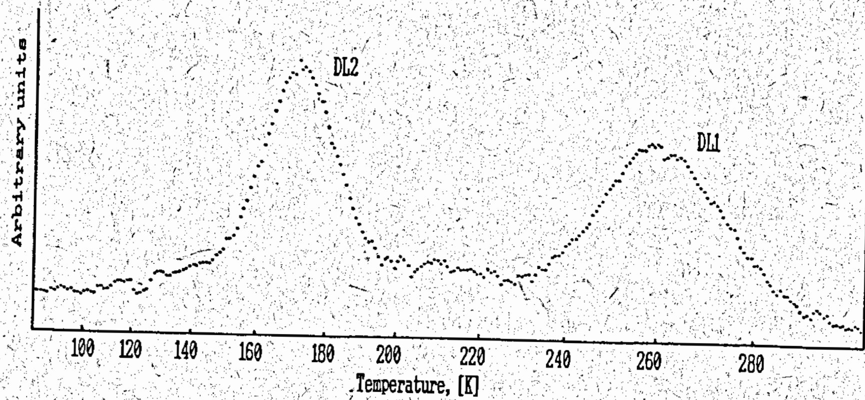

Fig.8 DLTS spectrum for the detector made of Wacker silicon.

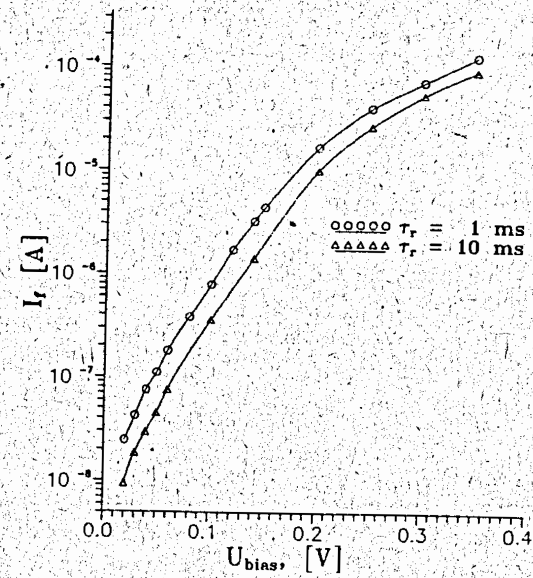

Fig.9 Forward current-voltage characteristics of the detectors from technological sets with different recombination lifetimes τ_r.

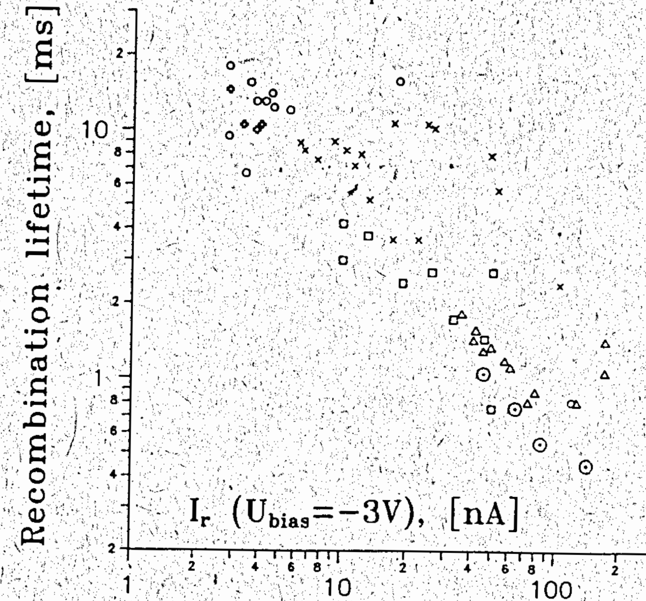

Fig.10 Dependence of the reverse current at bias voltage of 3V versus recombination lifetime τ_r.

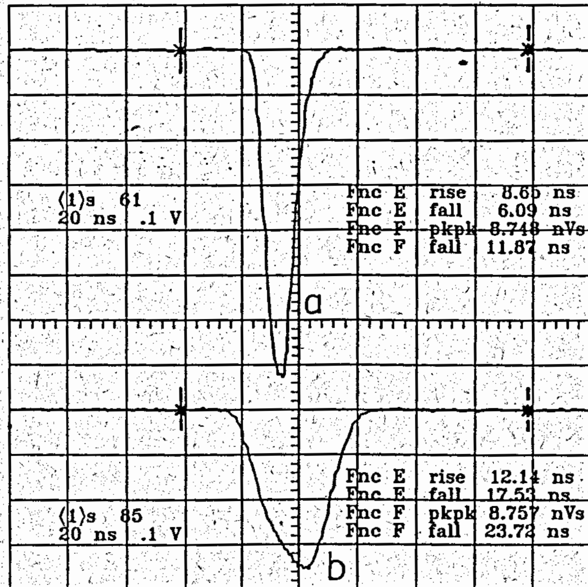

Fig.11 Curves of the current pulse response to: a,b – α-particle irradiation of p+ and n+ -layers, respectively; U_{bias} = 150 Volts.

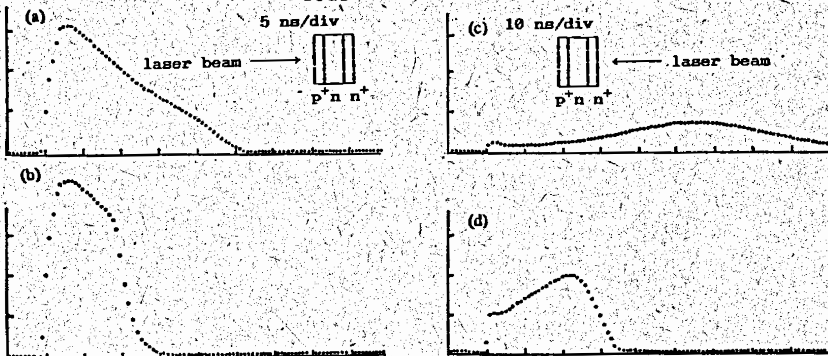

Fig.12 Curves of the current pulse response to light pulse excitation with duration of 0.7 ns at different bias voltages, namely:
a,b – the light pulse is absorbed near the p^+-layer;
c,d – the light pulse is absorbed near the n^+-layer;
Bias voltages: a,c – 70 V; b,d – 150 V.
Scale for light excitation response – 0.4 mA/div;
time: a,b – 5 ns/div; c,d – 10 ns/div.

Summary

The investigation results have shown that the technological process of the silicon planar detectors developed at ELMA, provides an effective gettering of the generation centres in high resistivity silicon. Indeed, the concentration of the deep levels is less than 10^9 cm^{-3} and the generation lifetime exceeds the initial value for as-grown silicon crystals. It allows to obtain the small reverse current and high lifetime of the charge carriers. The detectors can be successfully applied in high energy physics as well as in the traditional spectroscopy.

In conclusion we would like to express our acknoledgement to F.Lemeilleur (CERN) for his help in measurements.

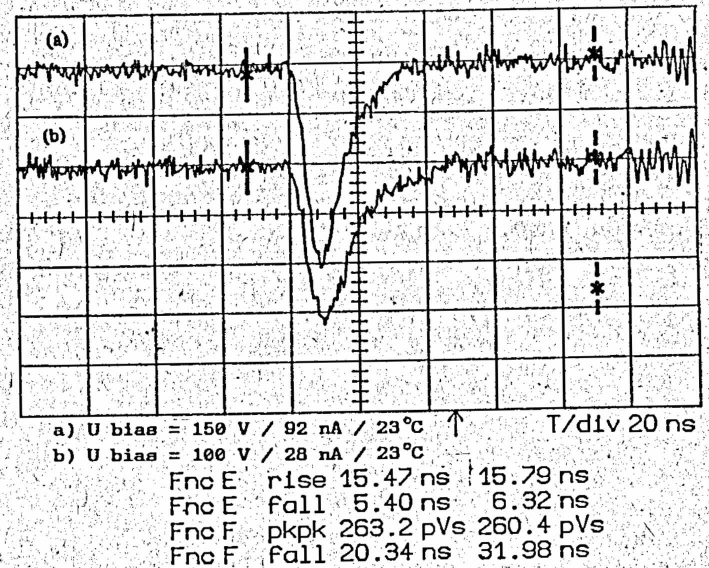

Fig.13 Curves of the current pulse response to m.i.p. excitation. Bias voltages:
a – 150 Volts, b – 100 Volts.

References

1. Design Study of the Large Hadron Collider, CERN 91-03.
2. R. Wunstorf, M. Benkert, N. Claussen, N. Croitoru, E. Fretwurst, G. Lindström and T. Schulz, Nucl. Instr. and Meth., A315 (1992) 149.
3. H.W. Kraner, Z. Li, Nucl. Instr. and Meth., A279 (1989) 266.
4. E. Borchi, C. Bertrand, M. Bruzzi, C. Furetta, P. Giubellino, C. Leroy, R. Paludetto, P.-G. Rancoita and L. Vismara, Nucl. Instr. and Meth. A279 (1989) 277.
5. V.V. Voronkov, J. Crystal Growth 1982, 59 (1982) 625.
6. A.A. Sitnikova, L.M. Sorokin et al., Phys. Stat. Solidi, A81 (1984) 433.
7. C.T. Sah and C.T. Wang, J. Appl.Phys., 46 (1975) 1767.
8. E.M. Verbitskaya, V.K. Eremin, A.M. Ivanov and N.B. Strokan, Sov. Phys. Semicond., 26 (1992) 1962.
9. E.M. Verbitskaya, V.K. Eremin, N.B. Strokan, J.von Borany, B. Schmidt, Nucl. Instr. and Meth., A281 (1989) 167.
10. E.M. Verbitskaya, V.K. Eremin, A.M. Malyarenko, N.B. Strokan, V.L. Sukhanov, J. Borany and B.Schmidt, Prib. Tekh. Eksp., N3 (1991) 56.
11. A.A.Quaranta, A.Taroni, G.Zanarini, IEEE Trans. Nucl. Sci., NS-15 (1968) 373.

Received by Publishing Department
on July 1, 1994.